The Mid-Pleistocene Record of Ice-Rafting at IODP Site 1308, Central North Atlantic: Links Between IRD Abundance Variations and Climatic Transitions

Senior Thesis

Submitted in partial fulfillment of the requirements for the
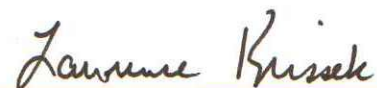
Bachelor of Science Degree

At The Ohio State University

By

Michael Victor Kellum

The Ohio State University

2015

Approved by

Lawrence A. Krissek, Advisor

School of Earth Sciences

Table of contents

Abstract

This project examines sediment samples from IODP Site 1308 in the central North Atlantic to reveal details about the history of glacial fluctuations from 292 thousand years ago (kya) to 525 kya. The project is based on a compositional analysis of 65 sand-fraction samples, taken at a sampling interval of ~ 3600 years. The sediment compositions are used to identify potential sources, thereby defining the areas of glacial fluctuations on adjacent landmasses.

Samples were examined using a binocular microscope to determine sediment composition and component abundances. Sample ages were assigned using a published oxygen isotope stratigraphy for Site 1308, and ages were then correlated to Marine Isotope Stages (MIS), which catalog alternating warm and cool periods in the Earth's paleoclimate, with even-numbered stages representing glacial periods and odd-numbered stages representing warm interglacial periods.

This study reveals that the relative abundance records of ice-rafted debris (IRD) and biogenic components (foraminifers) can be subdivided into 4 intervals, defined by fairly regular variations in the relative abundances of these two components. Within the IRD component, variations in the relative abundances of quartz and fine-grained mafic rock fragments are consistent with the 4 intervals defined by variations in the relative abundance of IRD overall. IRD generally is more abundant during glacial stages and during stage

transitions. This relationship is illustrated well within MIS 12 and during the MIS 12/11 transition. However, IRD is also abundant during some interglacials, indicating that IRD supply to this location in the North Atlantic is not controlled solely by global climate state.

Acknowledgements

Introduction

The longest and most complete records of continental glaciation are often acquired from stratigraphically intact deep marine sedimentary sequences. Ice-rafting is the transport of land-derived sediments by icebergs in mid and high latitude marine settings. These icebergs eventually melt and release those sediments to the seafloor as they drift into warmer seas (St. John et al, 2004). These sediments are known as ice-rafted debris (IRD). IRD abundance is a very useful proxy for gaining an understanding of glacial activity, such as glacial expansion to sea level, and IRD composition can be used to identify glaciated areas.

IRD records also have some limitations when determining ice sheet changes over long periods of time. While continuous marine deposition in deep marine settings offers high preservation potential for long term IRD records, factors other than ice sheet changes can influence this record (St. John et al, 2004). The distance from the depositional site is to its possible IRD sources is an important factor in determining the possible effects of other sources on the IRD record. The increased distance from a possible source allows for the chance of more mixing from other sediment sources. Changing surface currents may affect the iceberg dispersal patterns, independent of changes in the distribution of continental ice. Changes in sea-surface temperature patterns can affect the rate and position of IRD melt-out, which can further complicate a proxy record that is being interpreted for long-term changes in ice

sheet volume and location. The objective of this study is to define and interpret the history, sources, and controls on ice-rafting in the central North Atlantic during the mid Pleistocene (Marine Isotope Stages 8-13). For this study, IRD is defined as the lithic grains in the sand fraction between 150 μm and 2mm in diameter.

Geologic Setting

This study examines the IRD record in samples from IODP Site 1308 (Figure 1). Site U1308 constitutes a reoccupation of DSDP Site 609 (Figures 2 & 3), which provided material for very important studies of benthic $\delta^{18}O$, $\delta^{13}C$, and $CaCO_3$ records for the Pleistocene (Ruddiman et al., 1989) and late Pliocene (Ruddiman et al., 1986; Raymo et al., 1989).

The importance of Site 609 to the study of IRD was emphasized by the early identification of detrital-rich (Heinrich-type) layers based on lithic counts (Broecker et al., 1992; Bond et al., 1992). Heinrich events are sediment layers rich in IRD and poor in foraminifera. Petrologic characteristics of the IRD at Site 609 (Bond and Lotti, 1995) showed that Heinrich events are superimposed on another, higher-frequency rhythm of ice-rafting events with detrital sources not only in Hudson Strait but also in Greenland, Iceland, and Europe (Snoeckx et al., 1999; Grousset et al., 2000).
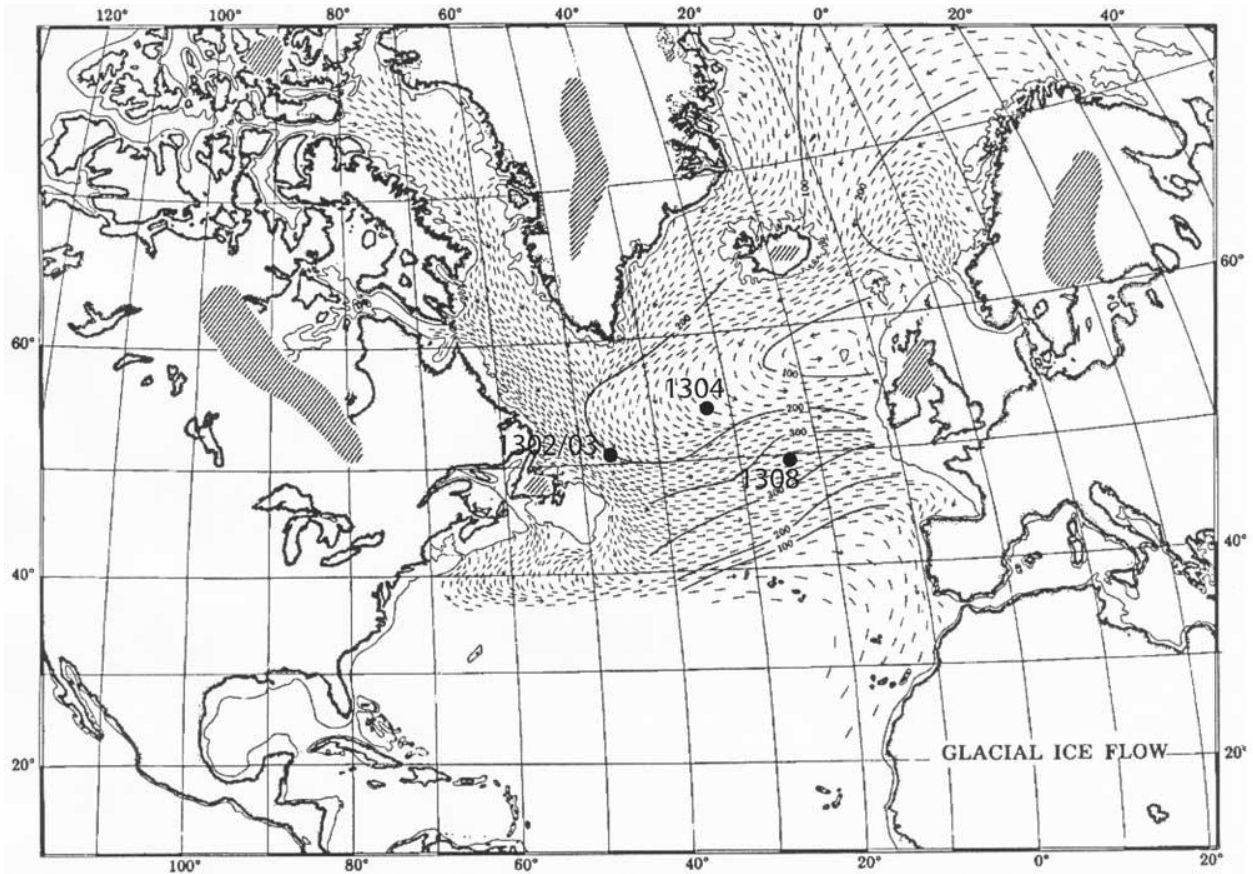
Figure 1. Position of IODP Sites U1302/03, U1304, and U1308 relative to IRD accumulation for the last glaciation (modified after Ruddiman [1977]). Arrows represent mean paths of distributions of ice-rafted debris during glacial periods inferred by Ruddiman (1977).

Studies of material from DSDP Site 609 have played a major role in driving some of the most exciting developments in paleoceanographic research during the early 21st century, such as the recognition and understanding of Heinrich layers (Channell et al., 2004). During Heinrich events, armadas of icebergs calved from glaciers and traversed the North Atlantic. The icebergs contained rock fragments eroded by the glaciers, and as they melted, these fragments were dropped onto the sea floor as IRD. Heinrich events are the

climatic events causing at least some of the IRD layers observed in marine sediment cores from the North Atlantic (Channell et al. 2004). Some IRD is not in Heinrich layers; especially farther back in time, the classic Heinrich-type event model may not apply.
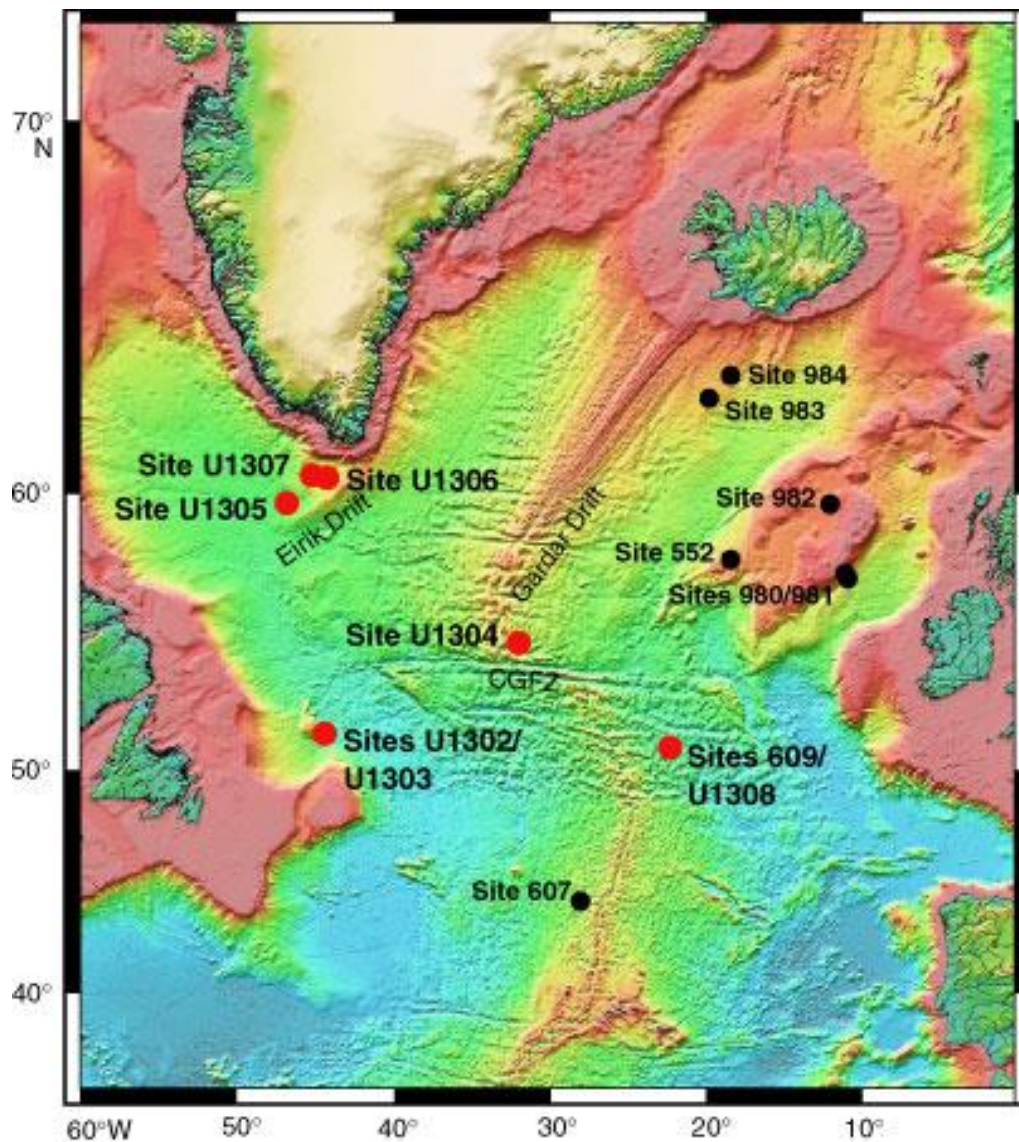
Figure 2. Location of Expedition 303 sites (red) and other Deep Sea Drilling Project (DSDP) and Ocean Drilling Program (ODP) sites mentioned in the text. CGFZ = Charlie Gibbs Fracture Zone. (Expedition 303 Scientists, 2006).
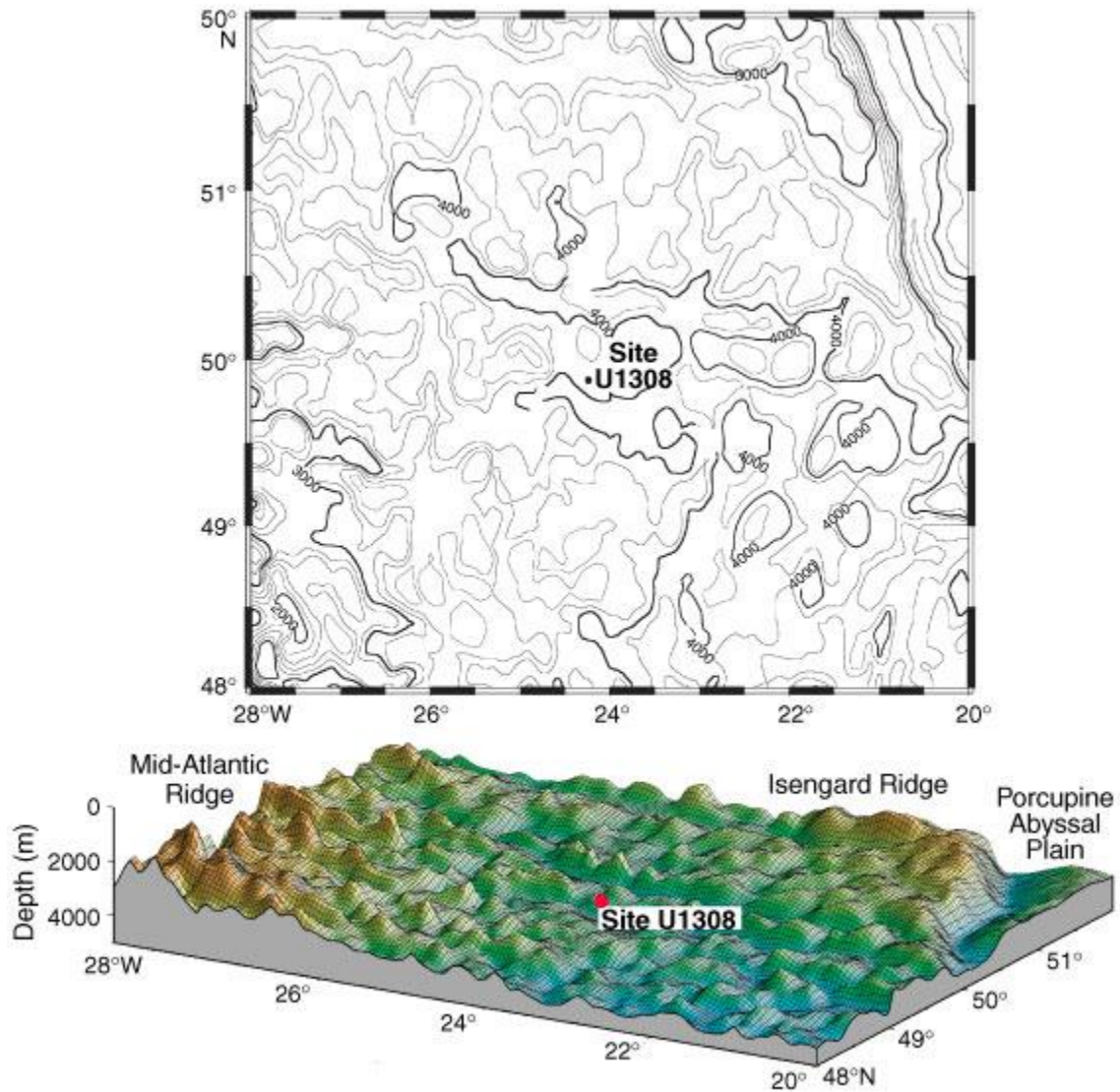
Figure 3. Location of Site U1308 lying between the eastern side of the mid-oceanic ridge (to the southwest) and the Isengard Ridge and Porcupine Abyssal Plain (to the northeast). Bathymetry from Smith and Sandwell (1994). Figure from Expedition 303 Scientists (2006).

Marine Isotope Stages (MIS) are alternating warm and cool periods in the Earth's paleoclimate during the Neogene, deduced from oxygen isotope compositions of foraminiferal calcite; these Marine Isotope Stages reflect

changes in global ice volume and ocean temperature. Working backwards from the present, MIS 1 is the present interglacial; stages with even numbers represent cold glacial periods, while the odd-numbered stages represent warm interglacial intervals. Other sedimentary records then can be compared with the MIS data and can be used to identify other changes in paleoclimates and paleoenvironments.

Many potential sources of IRD are exposed around the North Atlantic; their locations and geology have been summarized by a number of investigators (e.g., Krissek and St. John, 2002; Peck et al., 2007; Whyte, 2014). Potential sources of IRD for this study include silicic igneous and metamorphic basement rocks from Canada, central eastern Greenland, and southern Greenland. The basic igneous rocks could have been supplied from Iceland and central eastern Greenland (Tertiary volcanic province). Krissek and St. John (2002) studied ice rafted debris off the coast of southeast Greenland and concluded that the source of the basaltic IRD was central east Greenland. St. John et al. (2004) studied ice rafted debris off southeast Greenland and concluded that volcanic glass found in the IRD originated from Iceland; they also concluded that basaltic IRD could have originated from Iceland as well as from Greenland. Carbonate rock fragments as IRD are generally attributed to icebergs coming from the Hudson Bay region (Whyte 2014). This very distinctive IRD composition has been a major reason that the short-duration ice-rafting episodes called "Heinrich events" have generally been interpreted to record rapid collapses of the Laurentide Ice Sheet. Fe-stained quartz is attributed to

Paleozoic sediments also exposed in southern/eastern Canada, or to Mesozoic sediments in coastal southeastern Greenland.

Methods

The studied stratigraphic interval from Site 1308 was 16.2 meters long, and extended from 18.74 to 33.94 meters composite depth (MCD). Sixty-five samples were analyzed. The average time spacing between samples is estimated at 3,600 years. Prior to this study, samples had been sieved at grain sizes of 150 μm and 2mm. The present study involved visual inspection of the 150 μm–2mm size fraction, using a binocular microscope to determine grain compositions and abundances. From each sample, a subsample was poured into an aluminum weighing boat, and was examined using the binocular microscope. Through the microscope 100 grains were counted in each sample, and were categorized by composition. Replicate analyses were performed; this was done by recounting a few of the early samples in order to determine analytical uncertainty. These analyses showed that there was little uncertainty in the categorization of grain types from the samples. Multiple counts from the same sample were consistent.

The grain categories identified were as follows: Quartz (**Qtz**), Iron-stained Quartz (**Fe-Qtz**), Quartzose rock fragments (**QRF**) (Granites/Gneisses), Coarse grained mafic rock fragments (**CGM**) (Gabbros), Fine grained mafics (**FGM**)

(Basalts), Sedimentary rock fragments (**Sed Rocks)** (Sandstones & Shales), Carbonate rock fragments (**Carb Rocks**) (Limestones), Light and Dark Volcanic Ash (**Volc Ash D**) (**Volc Ash L**), Biogenic Silica (**Radiolarians**), Biogenic Carbonate (**Foraminifera**), Pyritic, and Other (**Mudballs**).

Profiles of component abundances vs. sediment age were constructed. This was done to illustrate compositional variations with age of the samples. Sample ages were determined using an age-depth model constructed by Hodell et al. (2008), based on an oxygen isotope stratigraphy. All values of the total terrigenous abundances were calculated using the following equation (terrigenous grains / terrigenous grains + biogenic silica and carbonates)*100. Many of the samples included other grains, primarily balls of mud that had not been disaggregated and removed as samples were processed; these additional grains were not categorized as IRD and were not included in the calculations of the total terrigenous abundances. Profiles of the component abundances vs. meters composite depth were constructed (Appendix B). The percentages of the individual IRD grain types were calculated using the following equation: (number of IRD grains of type X/total grains in the sample)*100. The percentages of the Qtz and FGM in Tables 1 and 2 were calculated using the following equation: (number of IRD grains of type X/ (total grains in the sample))*100.

Data

Two major grain types dominated the 150 μm–2mm size fraction at Site 1308: terrigenous grains (IRD) and biogenic carbonate (forams). The relative abundance profile of terrigenous IRD (Fig 4), and illustrates two intervals with relatively high IRD abundances and two intervals with relatively low abundances (Tables 1 & 2). The intervals with higher abundances occur at 310 to ~354 kya, and at 413 to 475 kya, whereas the intervals with relatively low IRD abundances span 355–413 kya and 475–513 kya (Table 1 & 2).

Within the terrigenous grain population, variations in the abundances of individual grain types also can be seen. The ice-rafted material is dominated by two major components, quartz and fine-grained mafic rock fragments (Figs. 6 & 7; also see Tables 1, 2, 3, and 4 in the Appendix A). The ice rafted material also contains lesser amounts of sedimentary rock fragments and quartzose fragments (Figs. 8 & 9). The quartz population shows significant abundance variation throughout the span of this study. The fine-grained mafic rock fragment population displays a more consistent record of abundance during several intervals lasting 30–70 ky. However, the fine-grained mafics also show large abundance variations in other parts of this record, sometimes changing from 0% to 100% in adjacent samples (Fig. 6).

The second major grain type is biogenic material, especially foraminifera (Figs. 10 and 11). Biogenic components are very common in deep sea sediments. At Site 1308, this population shows several intervals of relatively

9

consistent abundances throughout the studied time period. This population of biogenic grains dilutes the IRD component because the biogenic grains are relatively common, yet show large changes in their abundance. Extra care must be taken to properly distinguish the IRD from the biogenic components.
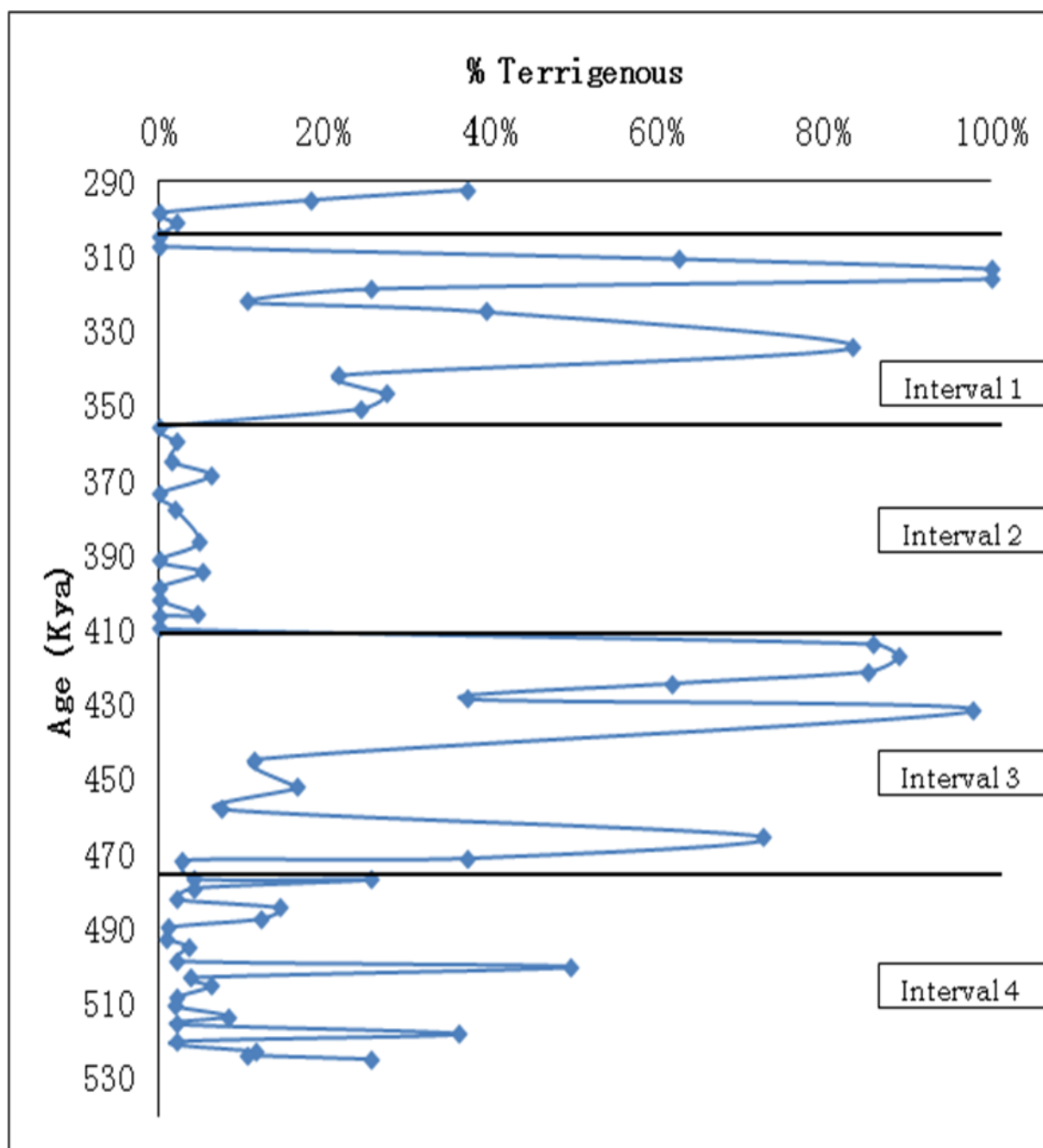
Figure 4. Abundances of total terrigenous grains found in the total sample, plotted with respect to age. This plot is subdivided into the 4 major intervals, based on relative abundance and variation patterns of the total terrigenous fraction. (Total terrigenous abundance is calculated as: ((the total number of terrigenous grains /(the total number of terrigenous + biogenic grains) *100))).
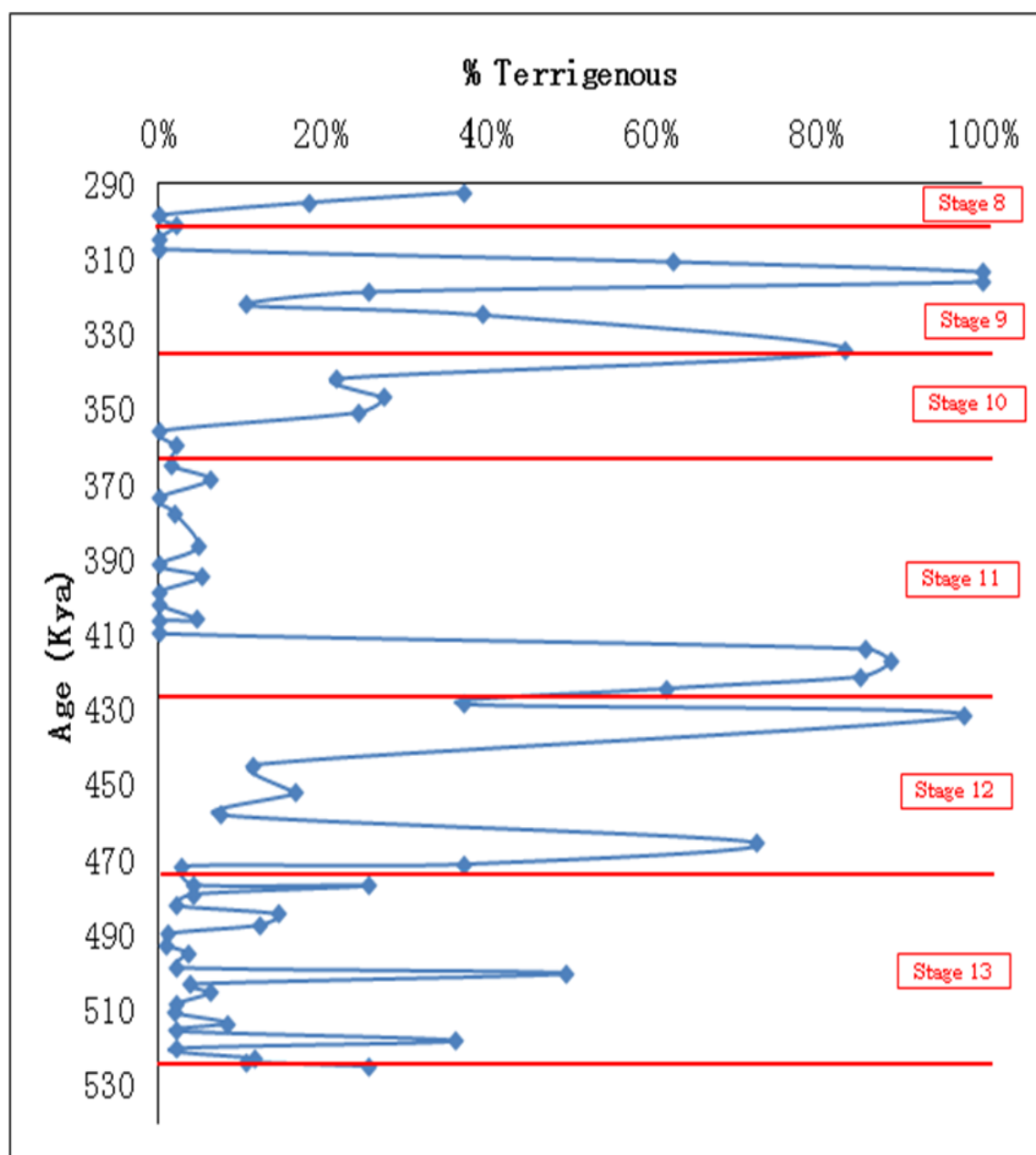
Figure 5. Abundances of total terrigenous grains relative to the total grain population, plotted with respect to age. This plot is overlaid with the Marine Isotope Stages.
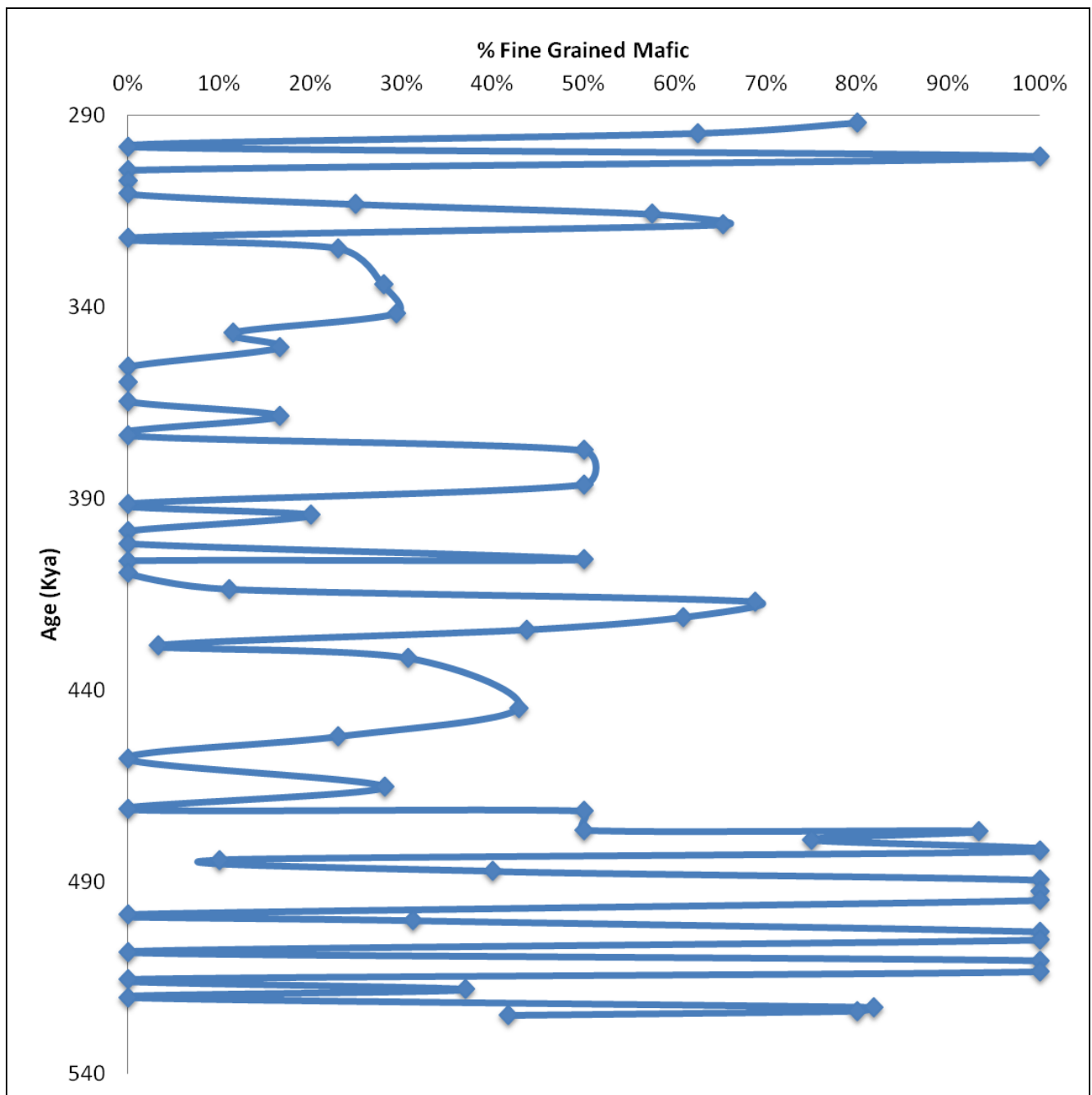
Figure 6. Abundance of Fine Grained Mafic grains relative to the total IRD grain population. The individual IRD grain types were calculated using the following equation: (number of IRD grains of type X / total IRD grains in that sample)*100.
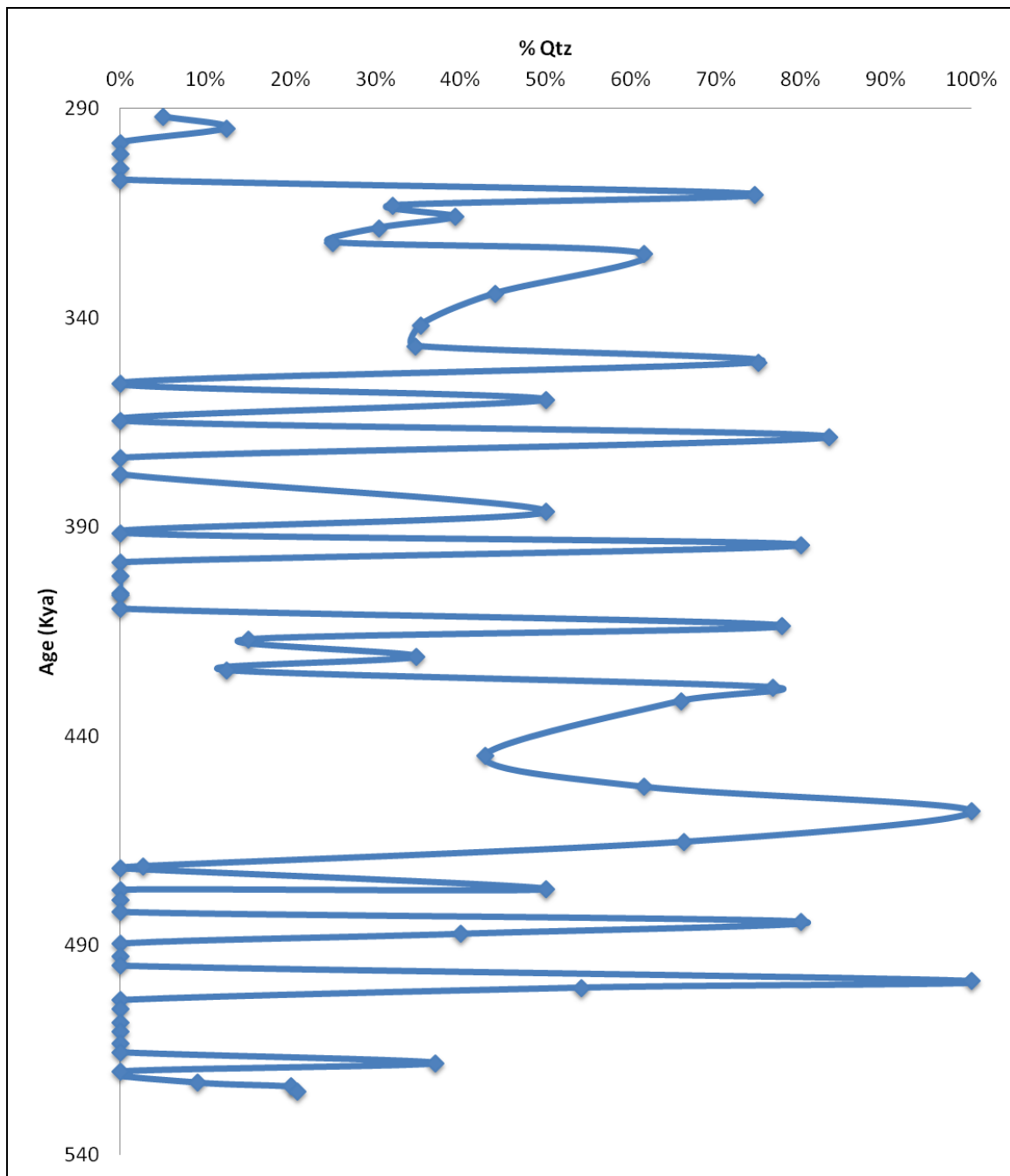
Figure 7. Abundance of Quartz grains relative to the total IRD grain population.
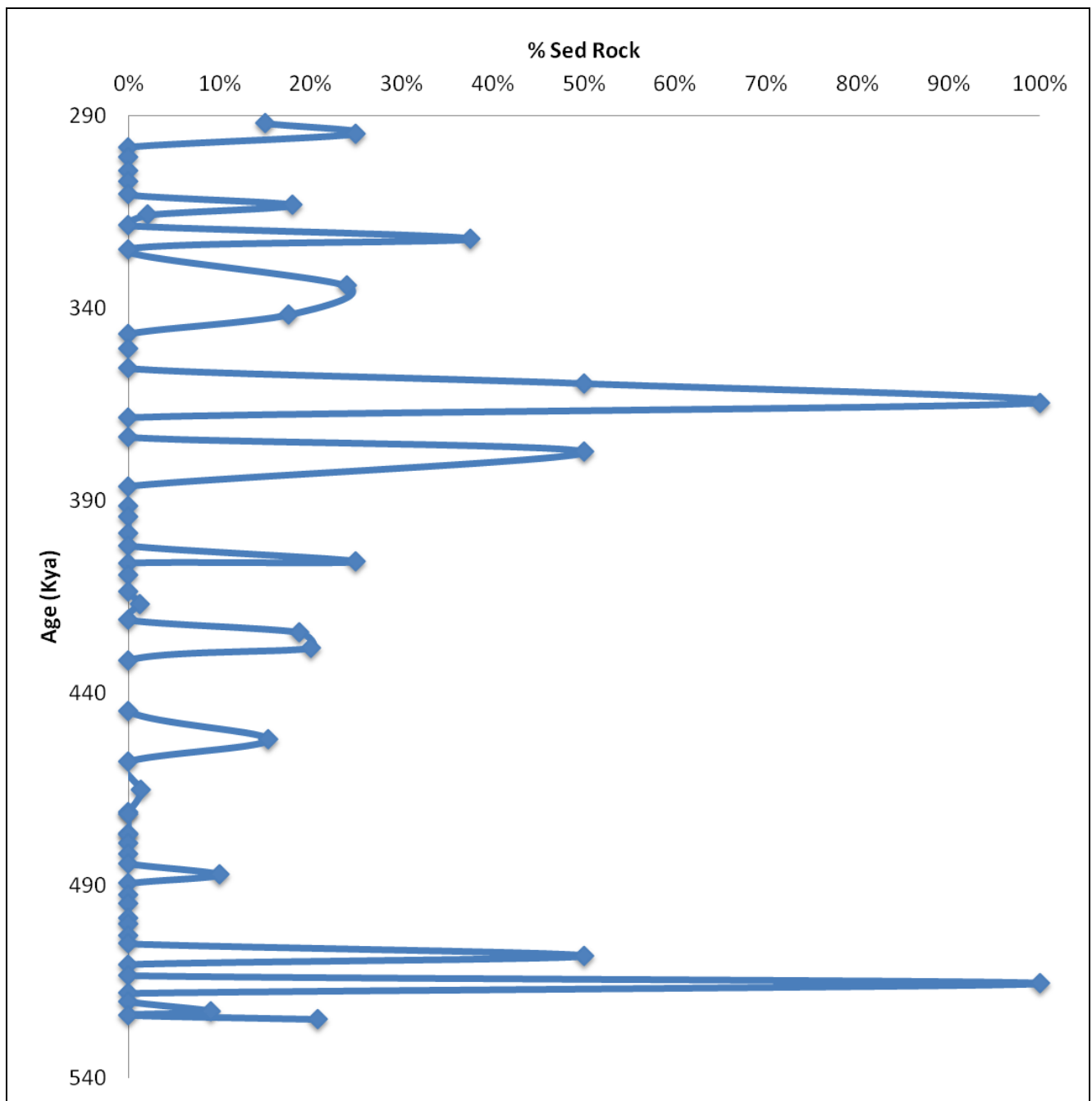
Figure 8. Abundance of Sedimentary Rock fragments relative to total IRD grains per sample.
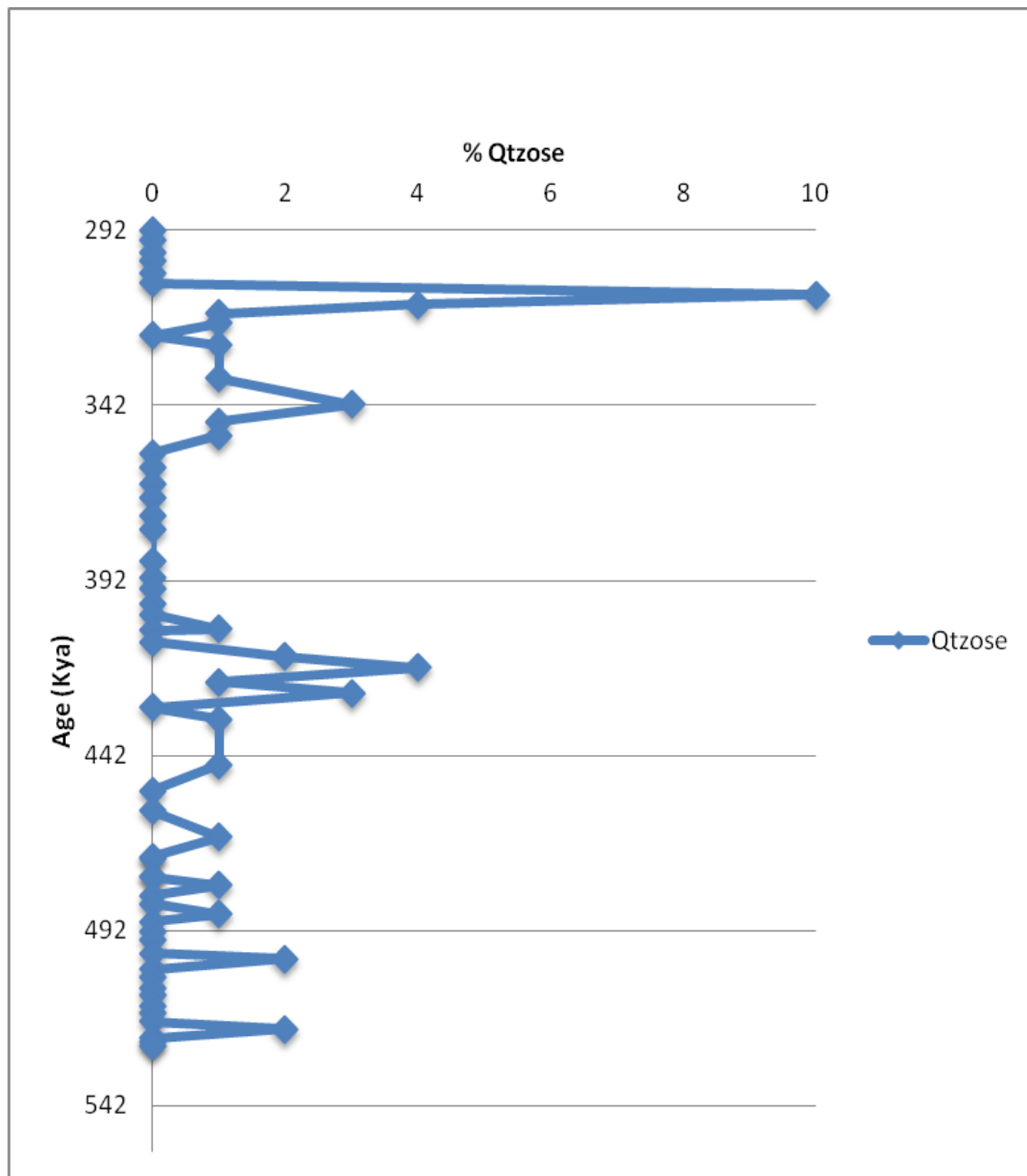
Figure 9. Abundance of Quartzose Rock fragments relative to total IRD grains per sample.
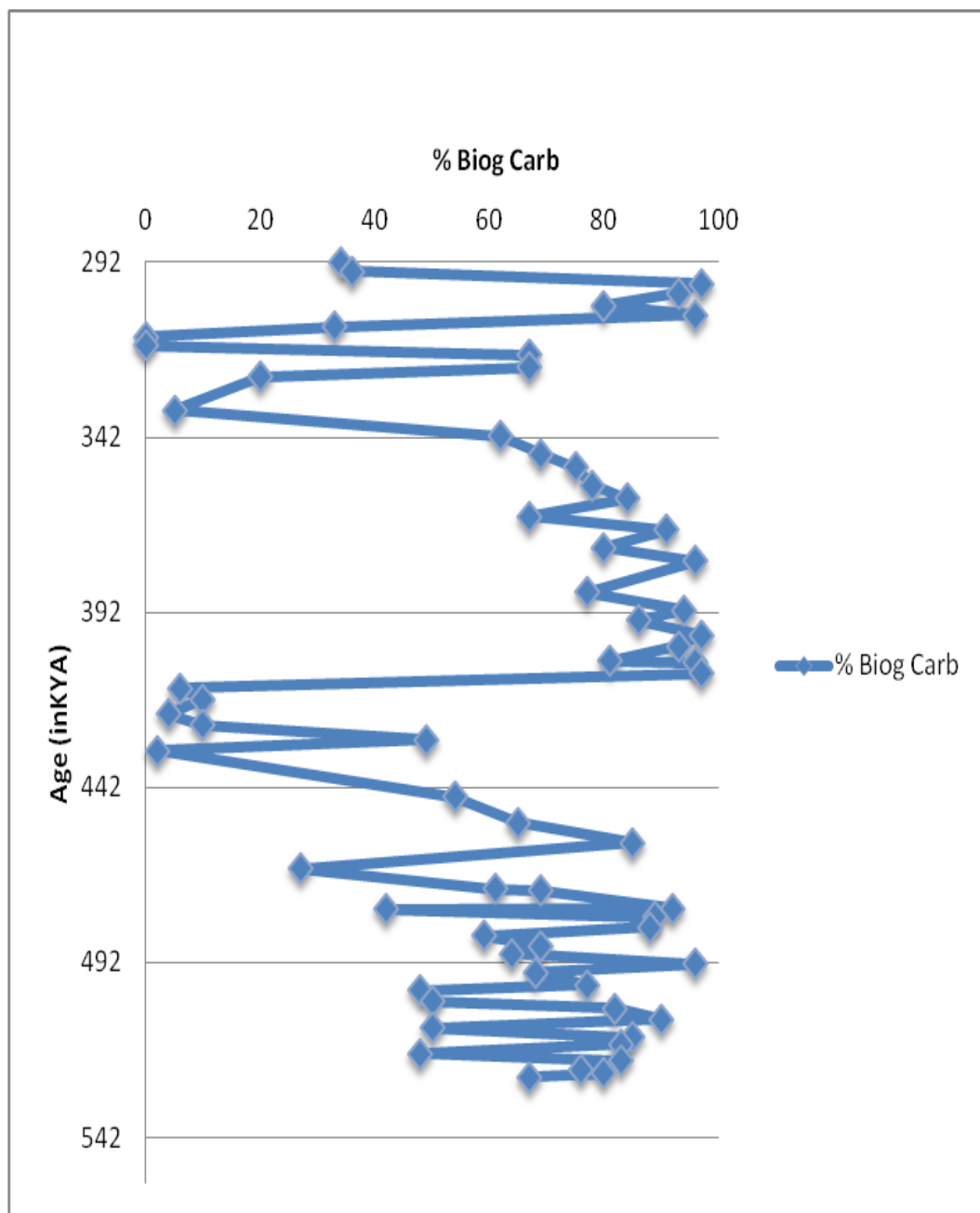
Figure 10. Abundance of biogenic carbonates relative to the total grain population.
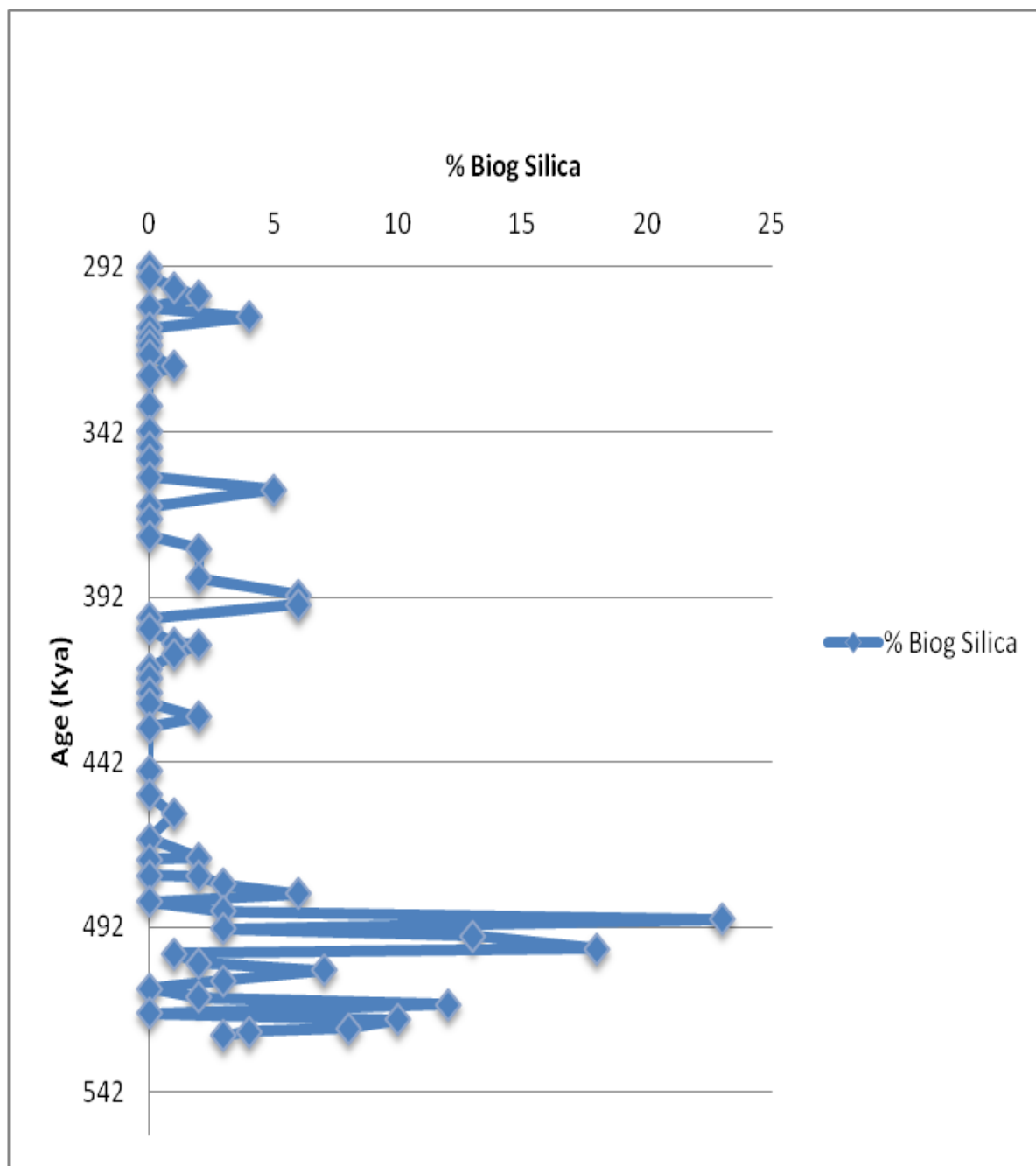
Figure 11. Abundance of biogenic silica relative to the total grain population.

Discussion

The data show that the samples from Site 1308 are dominated by two major grain types: terrigenous grains and biogenic grains. The abundance of total terrigenous grains is diluted by the variable presence of foraminifers, so that the abundance record of total terrigenous grains can be subdivided into four intervals with consistent patterns of variability (Fig. 4). The first interval, from 305 to 355 kya, averaged 41% total IRD with an average of 14.25% Qtz and 9.67% FGM. The second interval, from 355 to 410 kya, averaged only 2% IRD with an average of .92% Qtz and .54% FGM. The third interval, from 410 to 475 kya, averaged 50% IRD with 16.42% Qtz and 11.25% FGM. The fourth interval, from 475 to 525 kya, averaged only 10% IRD with 2.73% Qtz and 4.55% FGM (see Table 5). The percentages of the Qtz and FGM were calculated using the following equation: (number of IRD grains of type X /(total grains in the sample))*100. The biogenic components, the carbonates and the silica, make up the majority of the total grains found in most of the samples (Fig. 4).

The abundance of total terrigenous grains (i.e., IRD) can vary due to changes in controls on the IRD supply. These potential controls include changes in the IRD supply due to glacial/interglacial changes and to changes in iceberg transport paths and melting locations. Dilution by varying input and/or preservation of foraminifers could also affect the abundance record of IRD.

The total IRD record (Fig. 4) shows variations with some general links to the record of Marine Isotope Stages; however, these are not always strong and direct links. The warm interglacial periods tend to begin with a significant increase in IRD supply, followed by a significant decrease. This is well illustrated at the transition from Marine Isotope Stages 10 to 9. This relationship appears to be relatively similar to the transition from Stages 12 to 11. Two of the three interglacials (Stages 13 and 11) have relatively consistent low total IRD. Even though IRD abundances in Stage 9 are higher, both Stage 11 and Stage 9 show relatively high IRD abundances at the transition from the preceding glacial into that next interglacial. These are patterns that would be generally expected: less ice-rafting during warm interglacials, and decreasing IRD supply during times of glacial retreat. In both Stages 10 and 12, the IRD abundance generally increases as the glacial episode continues (i.e., from the base of 12 to the top of 12 and from the base of 10 to the top of 10). This pattern would be expected if ice extent increased through each glacial period.

The second major data set is the abundance of individual terrigenous grain types (Figs. 6, 7, 8, 9). Quartz and fine grained rock fragments make up a majority of the IRD grains. The other major components of the IRD include the quartzose and sedimentary rock fragments, and iron-stained quartz.

Each IRD grain type exhibits its own pattern of abundance variation over the interval studied. The quartz and fine grained rock fragment abundance patterns do not match in detail well, but both are generally similar to the

abundance pattern for the total IRD (Fig. 4). The quartz abundance record, however, generally shows larger and more frequent variations than the fine grain mafic rock fragment abundance record (Figs. 6 & 7). Sedimentary rock fragments and quartzose rock fragments are present sporadically, although QRF are more common when the overall IRD is more abundant (Figs. 8 & 9). A comparison of the records of total IRD and quartz suggests that increases in the total IRD generally were accompanied by relative increases in quartz abundances.

The two major components of the IRD, quartz and fine grained mafics, have several possible sources. The fine grained mafic rock fragments could have come from the central eastern Greenland area, which is a Tertiary volcanic province, or from Iceland. The quartz may have come from the central eastern Greenland province as well, but also may have been supplied from basement rocks in southern Greenland. Bedrock exposed in Canada also may have supplied quartz. The relatively similar timing of increased input of quartz and FGM suggests relatively synchronous ice expansion in multiple source areas, such as central eastern Greenland and/or Iceland, along with southern Greenland and/or eastern Canada. This finding is consistent with interpretations of an IRD record from Site 919 off southeast Greenland by Krissek and St. John (2002).

Conclusions

➢ The relative abundance records of IRD and biogenic components (foraminifers) from 292 to 525 kya at IODP Site 1308 can be subdivided into major 4 intervals, defined by relatively consistent patterns of variation in the relative abundances of these two components.

➢ The relative abundance of IRD is interpreted to have been controlled by variations in both the input rate of IRD and dilution by the input of foraminifers.

➢ Within the IRD component, the relative abundances of quartz and fine-grained mafic rock fragments are consistent with variations in the relative abundance of total IRD overall.

➢ The quartz abundance pattern follows the total IRD abundance pattern more closely than the FGM pattern does. This suggests that increases in total IRD were generally caused by an increase in quartz supply.

➢ The increase in quartz abundance may be due to variations in the IRD supply from Canada, where quartz does not co-occur with basalts, episodically superimposed on a more consistent supply of FGM-rich IRD from Iceland and East Greenland.

➢ Variations in the relative abundance of IRD do not correlate directly with Marine Isotope Stages. IRD generally is more abundant during glacial

stages and during stage transitions. This relationship is illustrated well within MIS 12 and during the MIS 12/11 transition (Fig. 5).

Suggestions for future work

Other studies in this region could include an analysis of older samples from Site 1308, a comparison of samples from other north Atlantic sites to analyze accuracy and /or large scale IRD activity, and an analysis of foraminifera found at Site 1308 could be done to further understand the ages of the samples and intervals in this study.

References

Bond, G., Heinrich, H., Broecker, W., Labeyrie, L.D., McManus, J., Andrews, J., Huon, S., Jantschik, R., Clasen, S., Simet, C., Tedesco, K., Klas, M., Bonani, G., and Ivy, S., 1992. Evidence for massive discharges of icebergs into the North Atlantic Ocean during the last glacial period. *Nature (London, U. K.),* 360:245–249. doi:10.1038/360245a0

Bond, G.C., and Lotti, R., 1995. Iceberg discharges into the North Atlantic on millennial time scales during the last glaciation. Science, 276:1005–1010.

Broecker, W.S., Bond, G.C., Mieczyslawa, K., Clark, E.A., and McManus, J., 1992. Origin of the northern Atlantic's Heinrich events. *In* Kelts, K.R. (Ed.), *Past and Present Climate Dynamics: Reconstruction of Rates of Change.* Clim. Dyn. 6(3–4):265–273. doi:10.1007/BF00193540

Channell, J.E.T., Sato, T., Kanamatsu, T., Stein, R., Malone, M.J., and the Expedition 303/306 Project Team, 2004. North Atlantic climate. IODP Sci. Prosp., 303/306. doi:10.2204/iodp.sp.303306.2004

Expedition 303 Scientists, 2006. Site U1308. *In* Channell, J.E.T., Kanamatsu, T., Sato, T., Stein, R., Alvarez Zarikian, C.A., Malone, M.J., and the Expedition 303/306 Scientists, *Proc. IODP,* 303: College Station TX (Integrated Ocean Drilling Program Management International, Inc.). doi:10.2204/iodp.proc.303306.108.2006

Grousset, F.E., Pujol, C., Labeyrie, L., Auffret, G., and Boelaert, A., 2000. Were the North Atlantic Heinrich events triggered by the behavior of the European ice sheets? Geology, 28:123–126. 2.3.CO;2"doi:10.1130/0091-7613(2000)028<0123:WTNAHE>2.3.CO;2

Hodell, David A, Channell, James E T, Curtis, Jason H, Romero, Oscar E,Rohl, Ursula,. PA4218 - onset of "Hudson Strait" Heinrich Events in the eastern North Atlantic at the end of the Middle Pleistocene Transition (-640 ka)? (DOI 10.1029/2008PA001591). Paleoceanography 2008;23(4):n.p.

Krissek, L.A., and St. John, K., 2002. Pleistocene iceberg production from East Greenland: synchronous between source areas, but distinct from global ice volume. Bulletin of the Geological Society of Denmark, 49, 79-89.

Peck, V. L., Hall, I. R., Zahn, R., Grousset, F., Hemming, S. R., and Sourse, J. D., 2007, The relationship of Heinrich events and their European precursors over the past 60 kyr BP: a multi-proxy ice rafted debris

provenance study in the Northeast Atlantic, Quaternary Science Reviews, 26, 862-875.

Raymo, M.E., Ruddiman, W.F., Backman, J., Clement, B.M., and Martinson, D.G., 1989. Late Pliocene variation in Northern Hemisphere ice sheets and North Atlantic deep water circulation. *Paleoceanography,* 4:413–446.

Ruddiman, W. F. (1977), Late Quaternary deposition of ice-rafted sand in the subpolar North Atlantic (lat 40 to 65N), Geol. Soc. Am. Bull., 88, 1813–1827, doi:10.1130/0016-7606(1977)88<1813:LQDOIS>2.0.CO;2.

Ruddiman, W.F., McIntyre, A., and Raymo, M., 1986. Matuyama 41,000 year cycles: North Atlantic Ocean and Northern Hemisphere ice sheets. *Earth Planet Sci. Lett.,* 80:117–129.

Ruddiman, W.F., Raymo, M.E., Martinson, D.G., Clement, B.M., and Backman, J., 1989. Pleistocene evolution: Northern Hemisphere ice sheet and North Atlantic Ocean. *Paleoceanography,* 4:353–412.

Snoeckx, H., Grousset, F., Revel, M., and Boelaert, A., 1999. European contribution of ice-rafted sand to Heinrich Layers H3 and H4. Mar. Geol., 158(1–4):197–208. doi:10.1016/S0025-3227(98)00168-6

Smith, W.H.F., and Sandwell, D.T., 1994. Bathymetric prediction from dense satellite altimetry and sparse shipboard bathymetry. *J. Geophys. Res.,* 99:21803–21824. doi:10.1029/94JB00988

St. John, K.E.K., B.P. Flower, and L. Krissek, 2004. Evolution of iceberg melt, biological productivity, and the record of Icelandic volcanism in the Irminger basin since 630 ka. Marine Geology, 212, 133-152.

Whyte, Colin, 2014 The Mid- to Late Pleistocene Ice Rafted Debris record at IODP Site 1308, Central North Atlantic. Unpublished B.S. Thesis, School of Earth Sciences, The Ohio State University: Columbus.

Appendix A

Age (Kya)	%Terrig	% Qtz	% FGM	MIS
305-355	41	14.25	9.67	9 + 10
355-410	2	0.92	0.54	10 + 11
410-475	50	16.42	11.25	11 + 12
475-525	10	2.73	4.55	13

Table 1. Avg % compositions by 4 intervals. Terrigenous (Terrig) is land-derived sediments. (Total terrigenous abundance is calculated as: ((the total number of terrigenous grains/ (the total number of terrigenous + biogenic grains) *100)).The percentages of the Qtz and FGM were calculated using the following equation: (number of IRD grains of type X /(total grains in the sample))*100.) Marine Isotope Stages (MIS) are identified for each interval.

MIS	Kya	Avg %Terrig	Avg % Qtz	Avg % FGM
8	292-301	7.5	0.5	5.75
9	301-334	35.33	15.33	11.56
10	334-364	11.67	5.67	2
11	364-427	11.73	4.07	5.8
12	427-474	31.88	18.83	6.88
13	474-524	8.86	2.73	4.55

Table 2 Avg % compositions by Marine Isotope Stages (MIS). Terrigenous (Terrig) is land-derived sediments. (Total terrigenous abundance is calculated as: ((the total number of terrigenous grains/ (the total number of terrigenous + biogenic grains) *100)).The percentages of the Qtz and FGM were calculated using the following equation: (number of IRD grains of type X/(total grains in the sample))*100.)

Sample							Abundance of Grains										Calculations					
Hole	Core	Section	Interval Top	Interval Bottom	MCD (meters composite depth)	Age (in KY)	Qtz	Fe-Qtz	Qtzose	Coarse Mafic	Fine Mafic	Sed Rock	Carb Rock	Volc Ash D	Volc Ash L	Pyritic	Terrig	Biog Carb	Biog Silica	Other	T + Bio	T /(T + Bio)
E	2	5	106	108	18.74	292.00	1				16	3					20	34		46	54	37%
E	2	5	128	130	18.96	294.72	1				5	2					8	36		56	44	18%
E	2	6	6	8	19.24	298.17											0	97	1	2	98	0%
E	2	6	28	30	19.46	300.89					2						2	93	2	3	97	2%
E	2	6	56	58	19.74	304.35											0	80		20	80	0%
E	2	6	78	80	19.96	307.06											0	96	4		100	0%
E	2	6	106	108	20.24	310.52	41	4	10								55	33		12	88	63%
E	2	6	128	130	20.46	313.23	32	3	4		25	18			18		100				100	100%
C	3	3	6	8	20.67	315.83	37		1		54	2					94			6	94	100%
C	3	3	28	30	20.89	318.54	7		1		15						23	67		10	90	26%
C	3	3	56	58	21.17	322.00	2					3		3			8	67	1	24	76	11%
C	3	3	78	80	21.39	324.72	8	1	1		3						13	20		67	33	39%
C	3	3	106	108	21.67	334.26	11		1		7	6					25	5		70	30	83%
C	3	3	128	130	21.89	341.71	6		3		5	3					17	62		21	79	22%
C	3	4	6	8	22.17	346.71	9		1		3			1	12		26	69		5	95	27%
C	3	4	28	30	22.39	350.64	18	1	1		4						24	75		1	99	24%
C	3	4	56	58	22.67	355.64											0	78		22	78	0%
C	3	4	78	80	22.89	359.57	1					1					2	84	5	9	91	2%
C	3	4	106	108	23.17	364.57						1					1	67		32	68	1%
C	3	4	128	130	23.39	368.50	5					1					6	91		3	97	6%
C	3	5	6	8	23.67	373.50											0	80		20	80	0%
C	3	5	28	30	23.89	377.43					1	1					2	96	2		100	2%
C	3	5	56	58	24.39	386.36	2				2						4	77	2	17	83	5%
C	3	5	78	80	24.67	391.36											0	94	6		100	0%

	Sample						Abundance of Grains										Calculations					
Hole	Core	Section	Interval Top	Interval Bottom	MCD (meters composite depth)	Age (in KY)	Qtz	Fe-Qtz	Qtzose	Coarse Mafic	Fine Mafic	Sed Rock	Carb Rock	Volc Ash D	Volc Ash L	Pyritic	Terrig	Biog Carb	Biog Silica	Other	T + Bio	T /(T + Bio)
C	3	5	128	130	24.89	394.35	4				1						5	86	6	3	97	5%
C	3	6	6	8	25.17	398.47											0	97		3	97	0%
C	3	6	28	30	25.39	401.71											0	93		7	93	0%
C	3	6	56	58	25.67	405.82			1		2	1					4	81	1	14	86	5%
E	3	2	56	58	25.7	406.26											0	96	2	2	98	0%
E	3	2	78	80	25.92	409.50											0	97	1	2	98	0%
E	3	2	106	108	26.2	413.62	28	2	2		4						36	6		58	42	86%
E	3	2	128	130	26.42	416.85	12	2	4		55	1		6			80	10		10	90	89%
E	3	3	6	8	26.7	420.97	8		1		14						23	4		73	27	85%
E	3	3	28	30	26.92	424.21	2	1	3		7	3					16	10		74	26	62%
E	3	3	56	58	27.2	428.32	23				1	6					30	49	2	19	81	37%
E	3	3	78	80	27.42	431.53	58	2	1		27						88	2		10	90	98%
E	3	3	128	130	27.92	444.68	3		1		3						7	54		39	61	11%
E	3	4	6	8	28.2	452.05	8				3	2					13	65		22	78	17%
E	3	4	28	30	28.42	457.84	7										7	85	1	7	93	8%
E	3	4	56	58	28.7	465.21	47	2	1		20	1					71	27		2	98	72%
E	3	4	78	80	28.92	471.00	1									36	37	61	2		100	37%
B	4	2	128	130	28.94	471.53					1				1		2	69		29	71	3%
E	3	4	106	108	29.2	476.47	2				2						4	92		4	96	4%
B	4	3	6	8	29.22	476.68					14					1	15	42	2	41	59	25%
B	4	3	28	30	29.44	479.00			1		3						4	89	3	4	96	4%
B	4	3	56	58	29.72	481.95					2						2	88	6	4	96	2%
B	4	3	78	80	29.94	484.26	8	1			1						10	59		31	69	14%
B	4	3	106	108	30.22	487.21	4		1		4	1					10	69	3	18	82	12%

Hole	Core	Section	Interval Top	Interval Bottom	MCD (meters composite depth)	Age (in KY)	Qtz	Fe-Qtz	Qtzose	Coarse Mafic	Fine Mafic	Sed Rock	Carb Rock	Volc Ash D	Volc Ash L	Pyritic	Terrig	Biog Carb	Biog Silica	Other	T + Bio	T /(T + Bio)
					Sample					Abundance of Grains									Calculations			
B	4	3	128	130	30.44	489.53					1						1	64	23	12	88	1%
B	4	4	6	8	30.72	492.47					1						1	96	3		100	1%
B	4	4	28	30	30.94	494.79					3						3	68	13	16	84	4%
B	4	4	56	60	31.29	498.47	2										2	77	18	3	97	2%
B	4	4	78	80	31.44	500.05	26	5	2		15						48	48	1	3	97	49%
B	4	4	106	108	31.72	503.00					2						2	50	2	46	54	4%
B	4	4	128	130	31.94	505.11					6						6	82	7	5	95	6%
B	4	5	6	8	32.22	508.26							1		1		2	90	3	5	95	2%
B	4	5	28	30	32.44	510.58					1						1	50		49	51	2%
B	4	5	56	58	32.72	513.37					8						8	85	2	5	95	8%
B	4	5	78	80	32.94	515.43						2					2	83	12	3	97	2%
B	4	5	106	108	33.22	518.05	10				10				4	3	27	48		25	75	36%
B	4	5	128	130	33.44	520.10			2								2	83	10	5	95	2%
B	4	6	6	8	33.72	522.72	1				9	1					11	76	8	5	95	12%
A	4	2	78	80	33.82	523.65	2				8						10	80	4	6	94	11%
B	4	6	28	30	33.94	524.78	5	1			10	5			2	1	24	67	3	6	94	26%

Table 3. Abundances of individual grain type data.

			Sample				% of Components												
Hole	Core	Section	Interval Top	Interval Bottom	MCD (meters composite depth)	Age (in KY)	Qtz	Fe-Qtz	Qtzose	Coarse Mafic	Fine Mafic	Sed Rock	Carb Rock	Volc Ash D	Volc Ash L	Biog Carb	Biog Silica	Pyritic	Other
E	2	5	106	108	18.74	292.00	1%	0%	0%	0%	16%	3%	0%	0%	0%	34%	0%	0%	46%
E	2	5	128	130	18.96	294.72	1%	0%	0%	0%	5%	2%	0%	0%	0%	36%	0%	0%	56%
E	2	6	6	8	19.24	298.17	0%	0%	0%	0%	0%	0%	0%	0%	0%	97%	1%	0%	2%
E	2	6	28	30	19.46	300.89	0%	0%	0%	0%	2%	0%	0%	0%	0%	93%	2%	0%	3%
E	2	6	56	58	19.74	304.35	0%	0%	0%	0%	0%	0%	0%	0%	0%	80%	0%	0%	20%
E	2	6	78	80	19.96	307.06	0%	0%	0%	0%	0%	0%	0%	0%	0%	96%	4%	0%	0%
E	2	6	106	108	20.24	310.52	41%	4%	10%	0%	0%	0%	0%	0%	0%	33%	0%	0%	12%
E	2	6	128	130	20.46	313.23	32%	3%	4%	0%	25%	18%	0%	18%	0%	0%	0%	0%	0%
C	3	3	6	8	20.67	315.83	37%	0%	1%	0%	54%	2%	0%	0%	0%	0%	0%	0%	6%
C	3	3	28	30	20.89	318.54	7%	0%	1%	0%	15%	0%	0%	0%	0%	67%	0%	0%	10%
C	3	3	56	58	21.17	322.00	2%	0%	0%	0%	0%	3%	0%	3%	0%	67%	1%	0%	24%
C	3	3	78	80	21.39	324.72	8%	1%	1%	0%	3%	0%	0%	0%	0%	20%	0%	0%	67%
C	3	3	106	108	21.67	334.26	11%	0%	1%	0%	7%	6%	0%	0%	0%	5%	0%	0%	70%
C	3	3	128	130	21.89	341.71	6%	0%	3%	0%	5%	3%	0%	0%	0%	62%	0%	0%	21%
C	3	4	6	8	22.17	346.71	9%	0%	1%	0%	3%	0%	0%	1%	12%	69%	0%	0%	5%
C	3	4	28	30	22.39	350.64	18%	1%	1%	0%	4%	0%	0%	0%	0%	75%	0%	0%	1%
C	3	4	56	58	22.67	355.64	0%	0%	0%	0%	0%	0%	0%	0%	0%	78%	0%	0%	22%
C	3	4	78	80	22.89	359.57	1%	0%	0%	0%	0%	1%	0%	0%	0%	84%	5%	0%	9%
C	3	4	106	108	23.17	364.57	0%	0%	0%	0%	0%	1%	0%	0%	0%	67%	0%	0%	32%
C	3	4	128	130	23.39	368.50	5%	0%	0%	0%	1%	0%	0%	0%	0%	91%	0%	0%	3%
C	3	5	6	8	23.67	373.50	0%	0%	0%	0%	0%	0%	0%	0%	0%	80%	0%	0%	20%
C	3	5	28	30	23.89	377.43	0%	0%	0%	0%	1%	1%	0%	0%	0%	96%	2%	0%	0%
C	3	5	78	80	24.39	386.36	2%	0%	0%	0%	2%	0%	0%	0%	0%	77%	2%	0%	17%
C	3	5	106	108	24.67	391.36	0%	0%	0%	0%	0%	0%	0%	0%	0%	94%	6%	0%	0%
C	3	5	128	130	24.89	394.35	4%	0%	0%	0%	1%	0%	0%	0%	0%	86%	6%	0%	3%
C	3	6	6	8	25.17	398.47	0%	0%	0%	0%	0%	0%	0%	0%	0%	97%	0%	0%	3%
C	3	6	28	30	25.39	401.71	0%	0%	0%	0%	0%	0%	0%	0%	0%	93%	0%	0%	7%
C	3	6	56	58	25.67	405.82	0%	0%	1%	0%	2%	1%	0%	0%	0%	81%	1%	0%	14%
C	3	2	56	58	25.7	406.26	0%	0%	0%	0%	0%	0%	0%	0%	0%	96%	2%	0%	2%
C	3	2	78	80	25.92	409.50	0%	0%	0%	0%	0%	0%	0%	0%	0%	97%	1%	0%	2%
C	3	2	106	108	26.2	413.62	28%	2%	2%	0%	4%	0%	0%	0%	0%	6%	0%	0%	58%
C	3	3	128	130	26.42	416.85	12%	2%	4%	0%	55%	1%	0%	6%	0%	10%	0%	0%	10%
C	3	3	6	8	26.7	420.97	8%	0%	1%	0%	14%	0%	0%	0%	0%	4%	0%	0%	73%
C	3	3	28	30	26.92	424.21	2%	1%	3%	0%	7%	3%	0%	0%	0%	10%	0%	0%	74%
C	3	3	56	58	27.2	428.32	23%	0%	0%	0%	1%	6%	0%	0%	0%	49%	2%	0%	19%
C	3	3	78	80	27.42	431.53	58%	2%	1%	0%	27%	0%	0%	0%	0%	2%	0%	0%	10%

Sample							% of Components												
Hole	Core	Section	Interval Top	Interval Bottom	MCD (meters composite depth)	Age (in KY)	Qtz	Fe-Qtz	Qtzose	Coarse Mafic	Fine Mafic	Sed Rock	Carb Rock	Volc Ash D	Volc Ash L	Biog Carb	Biog Silica	Pyritic	Other
E	3	3	128	130	27.92	444.68	3%	0%	1%	0%	3%	0%	0%	0%	0%	54%	0%	0%	39%
E	3	4	6	8	28.2	452.05	8%	0%	0%	0%	3%	2%	0%	0%	0%	65%	0%	0%	22%
E	3	4	28	30	28.42	457.84	7%	0%	0%	0%	0%	0%	0%	0%	0%	85%	1%	0%	7%
E	3	4	56	58	28.7	465.21	47%	2%	1%	0%	20%	1%	0%	0%	0%	27%	0%	0%	2%
E	3	4	78	80	28.92	471.00	1%	0%	0%	0%	0%	0%	0%	0%	0%	61%	2%	36%	0%
B	4	2	128	130	28.94	471.53	0%	0%	0%	0%	1%	0%	0%	1%	0%	69%	0%	0%	29%
E	3	4	106	108	29.2	476.47	2%	0%	0%	0%	2%	0%	0%	0%	0%	92%	0%	0%	4%
B	4	3	6	8	29.22	476.68	0%	0%	0%	0%	14%	0%	0%	0%	1%	42%	2%	0%	41%
B	4	3	28	30	29.44	479.00	0%	0%	1%	0%	3%	0%	0%	0%	0%	89%	3%	0%	4%
B	4	3	56	58	29.72	481.95	0%	0%	0%	0%	2%	0%	0%	0%	0%	88%	6%	0%	4%
B	4	3	78	80	29.94	484.26	8%	1%	0%	0%	1%	0%	0%	0%	0%	59%	0%	0%	31%
B	4	3	106	108	30.22	487.21	4%	0%	1%	0%	4%	1%	0%	0%	0%	69%	3%	0%	18%
B	4	3	128	130	30.44	489.53	0%	0%	0%	0%	1%	0%	0%	0%	0%	64%	23%	0%	12%
B	4	4	6	8	30.72	492.47	0%	0%	0%	0%	1%	0%	0%	0%	0%	96%	3%	0%	0%
B	4	4	28	30	30.94	494.79	0%	0%	0%	0%	3%	0%	0%	0%	0%	68%	13%	0%	16%
B	4	4	58	68	31.29	498.47	2%	0%	0%	0%	0%	0%	0%	0%	0%	77%	18%	0%	3%
B	4	4	78	80	31.44	500.05	26%	5%	2%	0%	15%	0%	0%	0%	0%	48%	1%	0%	3%
B	4	4	106	108	31.72	503.00	0%	0%	0%	0%	2%	0%	0%	0%	0%	50%	2%	0%	46%
B	4	4	128	130	31.94	505.11	0%	0%	0%	0%	6%	0%	0%	0%	0%	82%	7%	0%	5%
B	4	5	6	8	32.22	508.26	0%	0%	0%	0%	0%	1%	0%	1%	0%	90%	3%	0%	5%
B	4	5	28	30	32.44	510.58	0%	0%	0%	0%	1%	0%	0%	0%	0%	50%	0%	0%	49%
B	4	5	56	58	32.72	513.37	0%	0%	0%	0%	8%	0%	0%	0%	0%	85%	2%	0%	5%
B	4	5	78	80	32.94	515.43	0%	0%	0%	0%	0%	2%	0%	0%	0%	83%	12%	0%	3%
B	4	5	106	108	33.22	518.05	10%	0%	0%	0%	10%	0%	0%	0%	4%	48%	0%	3%	25%
B	4	5	128	130	33.44	520.10	0%	0%	2%	0%	0%	0%	0%	0%	0%	83%	10%	0%	5%
B	4	6	6	8	33.72	522.72	1%	0%	0%	0%	9%	1%	0%	0%	0%	76%	8%	0%	5%
A	4	2	75	80	33.82	523.65	2%	0%	0%	0%	8%	0%	0%	0%	0%	80%	4%	0%	6%
B	4	6	28	30	33.94	524.78	5%	1%	0%	0%	10%	5%	0%	2%	1%	67%	3%	0%	6%

Table 4. % Abundances of individual grain types.

MCD	Age	Qtz	Avg % Qtz	Fe-Qtz	Qtzose	Coarse Mafic	Fine Mafic	Avg % FM	Sed Rock	Carb Rock	Volc Ash D	Volc Ash L	Pyritic	Terrig	Avg % Terrig	Biog Carb	Biog Silica	Other	T + Bio	T / T + Bio
18.74	292.00	1					16		3					20		34		46	54	37%
18.96	294.72	1					5		2					8		36		56	44	18%
19.24	298.17						0							0		97	1	2	98	0%
19.46	300.89	0					2							2		93	2	3	97	2%
19.74	304.35	0					0							0		80		20	80	0%
19.96	307.06	0					0							0		96	4		100	0%
20.24	310.52	41		4	10		0							55		33		12	88	63%
20.46	313.23	32		3	4		25		18		18			100					100	100%
20.67	315.83	37			1		54		2					94				6	94	100%
20.89	318.54	7			1		15							23		67		10	90	26%
21.17	322.00	2					0		3		3			8		67	1	24	76	11%
21.39	324.72	8		1	1		3							13		20		67	33	39%
21.67	334.26	11			1		7		6					25		5		70	30	83%
21.89	341.71	6			3		5		3					17		62		21	79	22%
22.17	346.71	9			1		3				1	12		26		69		5	95	27%
22.39	350.64	18		1	1		4							24		75		1	99	24%
22.67	355.64	0	14.25				0	9.67						0	41.20	78		22	78	0%
22.89	359.57	1					0		1					2		84	5	9	91	2%
23.17	364.57	0					0		1					1		67		32	68	1%
23.39	368.50	5					1							6		91		3	97	6%
23.67	373.50	0					0							0		80		20	80	0%
23.89	377.43	0					1		1					2		96	2		100	2%
24.39	386.36	2					2							4		77	2	17	83	5%
24.67	391.36	0					0							0		94	6		100	0%
24.89	394.35	4					1							5		86	6	3	97	5%
25.17	398.47	0					0							0		97		3	97	0%
25.39	401.71	0					0							0		93		7	93	0%
25.67	405.82	0			1		2		1					4		81	1	14	86	5%
25.7	406.26	0					0							0		96	2	2	98	0%
25.92	409.50	0	0.92				0	0.54						0	2.04	97	1	2	98	0%
26.2	413.62	28		2	2		4							36		6		58	42	86%
26.42	416.85	12		2	4		55		1		6			80		10		10	90	89%
26.7	420.97	8			1		14							23		4		73	27	85%
26.92	424.21	2		1	3		7		3					16		10		74	26	62%
27.2	428.32	23					1		6					30		49	2	19	81	37%

MCD	Age	Qtz	Avg % Qtz	Fe-Qtz	Qtzose	Coarse Mafic	Fine Mafic	Avg % FM	Sed Rock	Carb Rock	Volc Ash D	Volc Ash L	Pyritic	Terrig	Avg % Terrig	Biog Carb	Biog Silica	Other	T + Bio	T / T + Bio
27.42	431.53	58		2	1		27							88		2		10	90	98%
27.92	444.68	3			1		3							7		54		39	61	11%
28.2	452.05	8					3		2					13		65		22	78	17%
28.42	457.84	7					0							7		85	1	7	93	8%
28.7	465.21	47		2	1		20		1					71		27		2	98	72%
28.92	471.00	1					0						36	37		61	2		100	37%
28.94	471.53	0	16.42				1	11.25			1			2	50.45	69		29	72	4%
29.2	476.47	2					2							4		92		4	96	4%
29.22	476.68	0					14					1		15		42	2	41	59	25%
29.44	479.00	0			1		3							4		89	3	4	96	4%
29.72	481.95	0					2							2		88	6	4	96	2%
29.94	484.26	8		1			1							10		59		31	69	14%
30.22	487.21	4			1		4		1					10		69	3	18	82	12%
30.44	489.53	0					1							1		64	23	12	88	1%
30.72	492.47	0					1							1		96	3		100	1%
30.94	494.79	0					3							3		68	13	16	84	4%
31.29	498.47	2					0							2		77	18	3	97	2%
31.44	500.05	26		5	2		15							48		48	1	3	97	49%
31.72	503.00	0					2							2		50	2	46	54	4%
31.92	505.11	0					6							6		82	7	5	95	6%
32.22	508.26	0					0		1		1			2		90	3	5	95	2%
32.44	510.58	0					1							1		50		49	51	2%
32.72	513.37	0					8							8		85	2	5	95	8%
32.94	515.43	0					0		2					2		83	12	3	97	2%
33.22	518.05	10					10					4	3	27		48		25	75	36%
33.44	520.10	0			2		0							2		83	10	5	95	2%
33.72	522.72	1					9		1					11		76	8	5	95	12%
33.82	523.65	2					8							10		80	4	6	94	11%
33.94	524.78	5	2.94	1			10	4.59	5		2	1		24	9.41	67	3	6	94	26%

Table 5. Avg % composition data by 4 intervals (shown in purple).
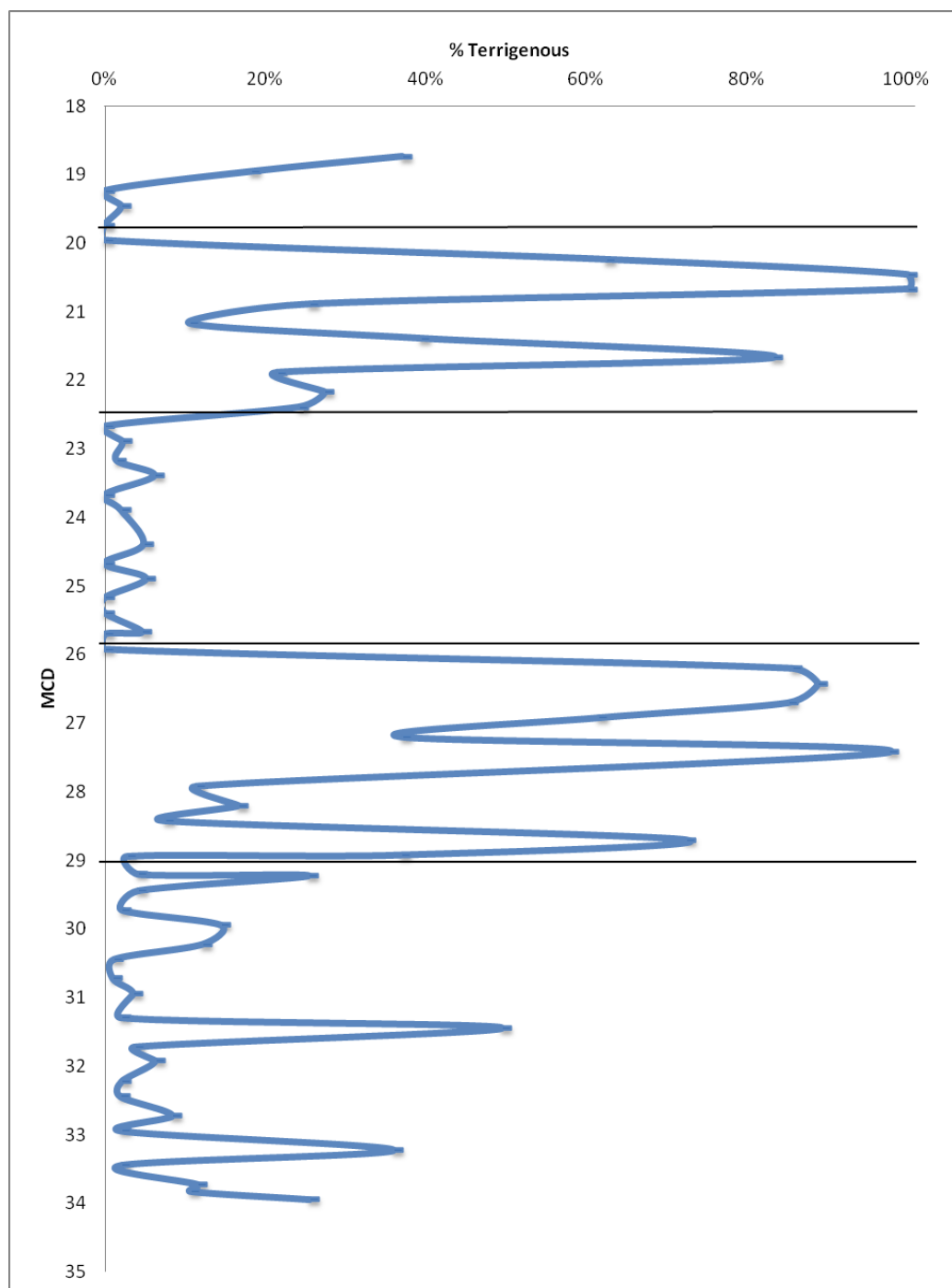
Appendix B

Figure 12. Plot showing the abundance of Terrigenous grains vs. MCD subdivided by the four major intervals.
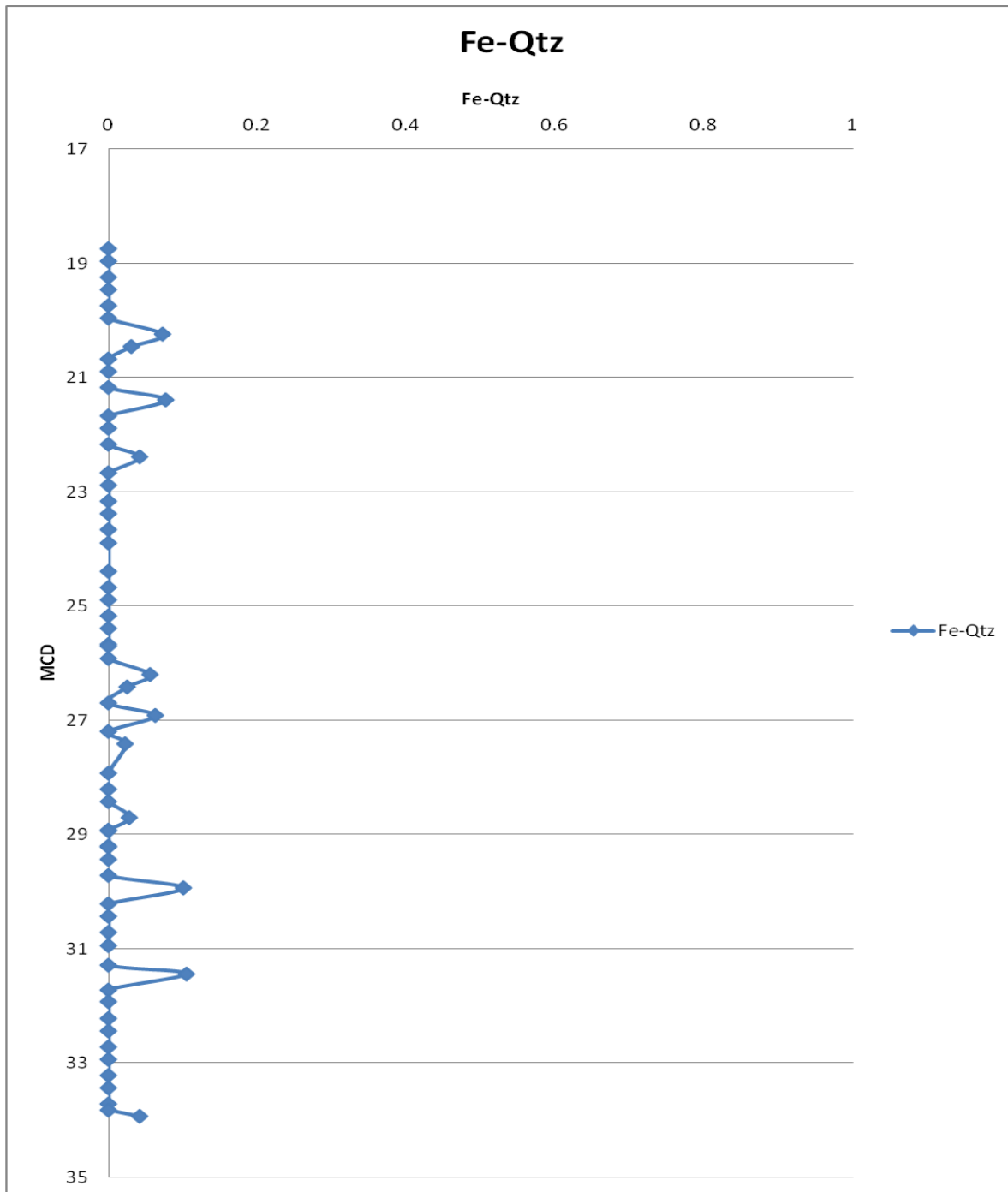
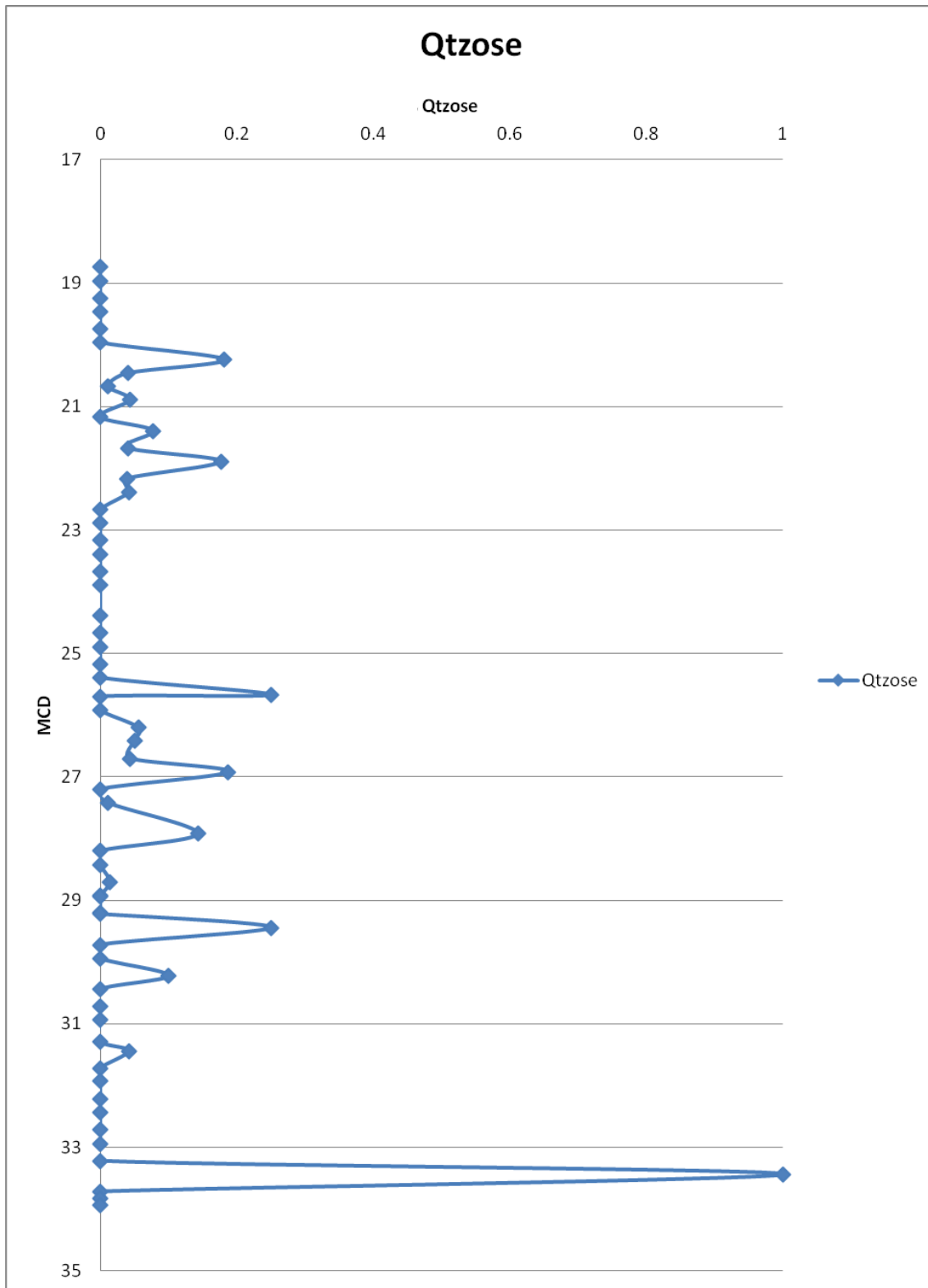**Figure 13.** Abundance of Fe-Qtz vs. MCD, relative to total IRD grains per sample.

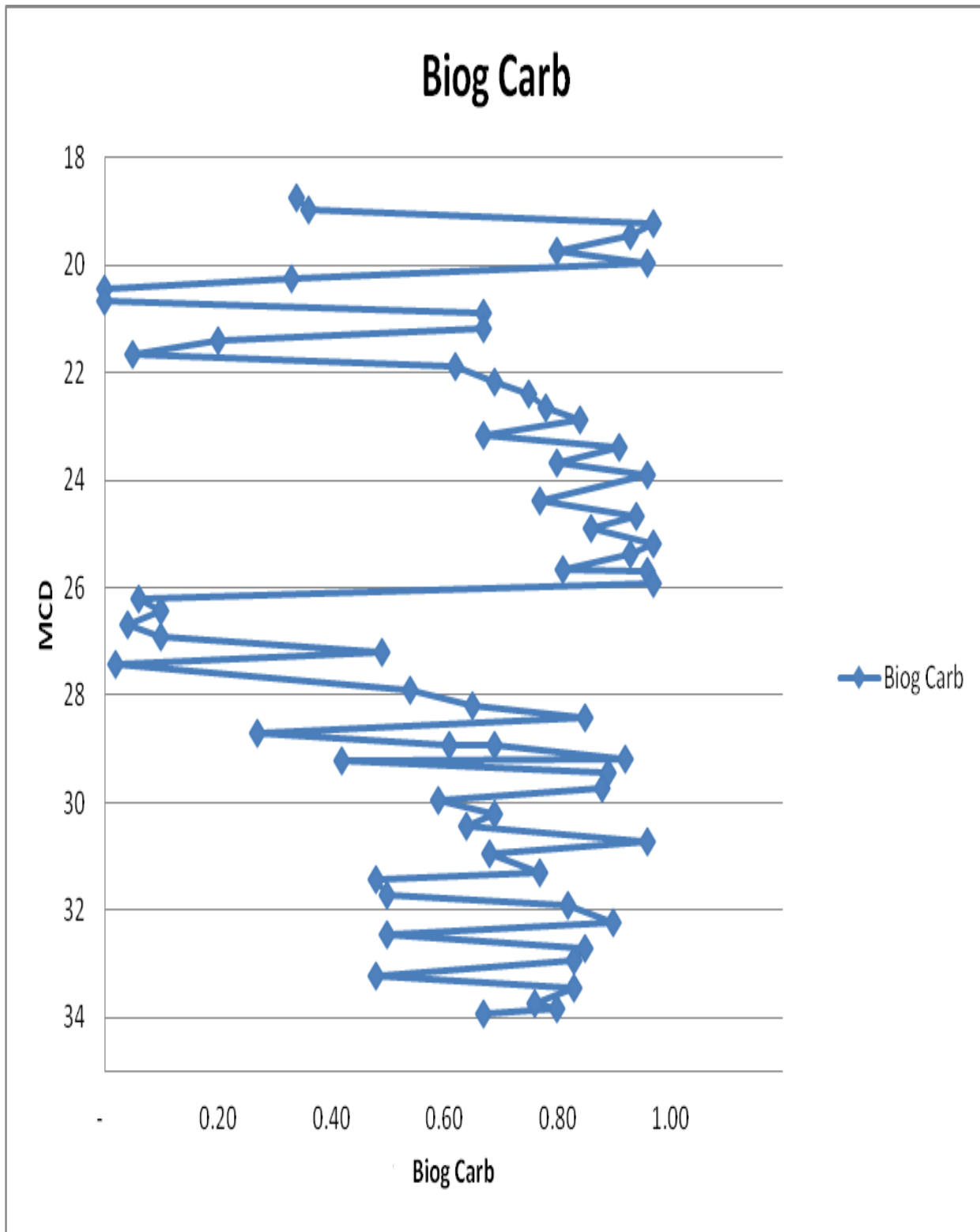**Figure 14.** Abundance of Qtzose vs. MCD, relative to total IRD grains per sample.
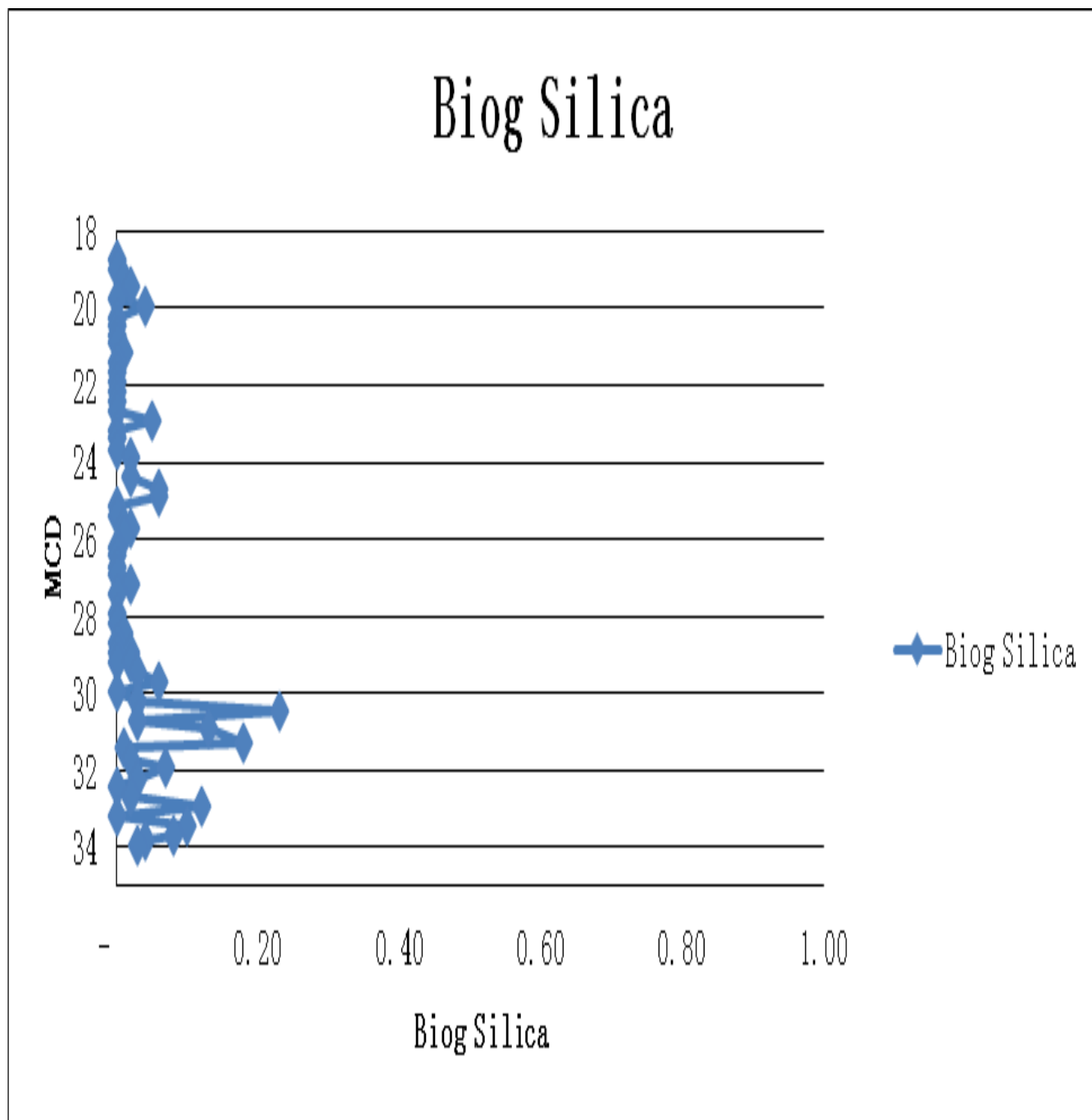
Figure 15. Biogenic Carbonates vs. All Grains.

Figure 16. Biogenic Silica vs. All Grains.